



Modified Reinforced Concrete Plane Stress Element Formulation for the Nonlinear Response of Seismic Resisting Systems

Abdel Khalik, A. K.¹; Hassan, H. M.² and Sallam, E. A.³

ABSTRACT

Design of economic seismic resisting structural systems with an acceptable safety margin requires continuous improvements for the available numerical models and analysis tools. In this work, an improved reinforced concrete membrane element based on the modified compression filed theory (MCFT) is presented. The developed element is implemented into a developed finite element program in order to study seismic response of different types of seismic resisting systems which are commonly used in the construction of concrete buildings in Egypt. Two types of floor systems, (beamed/beamless floors) and two types of seismic resisting systems, (frames/coupled frames with shear walls), are investigated. Reinforced concrete flexibility-based beam column and plane stress elements were used to model frames and shear walls, respectively. The static response of these systems subjected to triangular load pattern was investigated through nonlinear static analysis. It was concluded that, the predicted force reduction factor based on nonlinear static analysis of the examined systems is 50% to 75% less than those provided by Egyptian code; such variation could lead to uneconomic or inadequate design.

Keywords: Floor systems, RC frames, Shear walls, flexibility based, Plane Stress, Nonlinear, Static response.

1. Introduction

Determination of the structural properties (initial stiffness, ultimate capacity, and different global and local ductility demands) of a building is an essential step in the evaluation of its seismic response. Due to the complex interactions between various components of real structures, their nonlinear characteristics up to failure cannot be identified solely from the experimental tests of scale models. Historically these difficulties have been overcome by static tests on structural members or components on reduced-scale sub-assemblages of structures under cyclic load reversals.

Seismic resisting systems are commonly formed from either rigid frames or shear walls or dual systems composed from rigid frames and shear walls. From the various types of finite elements which are used in modeling of seismic resisting elements, two types are commonly investigated by researchers; beam-column and plane stress reinforced concrete elements. Modeling of reinforced concrete structural walls using plane stress elements have been studied by many researchers [1]. The modified compression filed theory (MCFT) gained popularity due its simplicity and ease of finite element implementation.

In 1990, finite element formulations for membrane elements are discussed in details [2]. Cracked reinforced concrete is treated as an orthotropic material based on smeared rotating crack model. Secant-stiffness moduli are defined for concrete and reinforcement, and these are used in the development of linear displacement rectangular and triangular membrane finite elements.

Hut proposed plane stress constitutive models for the nonlinear finite element analysis of reinforced concrete structures under monotonic loading [3]. An elastic strain hardening plastic stress-strain relationship with a nonassociated flow rule is used to model concrete in the compression dominating region and an elastic brittle fracture behavior is assumed for concrete in the tension dominating area. After cracking, the smeared cracked approach together with the rotating crack concept is employed. The reinforcement is modeled by an idealized bilinear curve identical in tension and compressions. In 1996, a static non-linear finite element analysis (FEM) followed by a non-linear dynamic analysis of lumped mass single degree of freedom model of the structure was proposed [4]. Jagd included in his model the nonlinear material behavior of concrete, rotating crack directions, sliding in old cracks and compressive strength reduction effects [4]. Hysteresis features that include stiffness degradation and pinching effects are also used to describe the cyclic behavior of the shear wall. The model was excellent for determining the dynamic behavior of shear wall with large concentrated mass [4].

Hidalgo developed a computer model capable of predicting the seismic behavior of shear-wall buildings [5]. The model allowed better estimations of both the

¹ Professor of Concrete Structures, Civil Engineering Department, Faculty of Engineering, Suez Canal University, Ismailia, Egypt

² Professor of Concrete Structures, Civil Engineering Department, Faculty of Engineering, Port Said University, Port Said, Egypt

³ PhD student, Civil Engineering Department, Faculty of Engineering, Port Said University, Port Said, Egypt

Email: Ezat_sallam@yahoo.com

ultimate lateral strength of these buildings as well as their inelastic deformation demand under severe ground motions. A shear failure mode model based on experimental results has been also added to the computer program. Mo presented the cyclic softened membrane model (CSMM) and implemented it into a finite element program, to predict the behavior of RC wall-type structures [6]. The entire hysteretic loops of framed shear walls, including the backbone curves, the initial stiffness, the yield point, the peak strength, the descending branch, the failure characteristics, the pinching effect, the residual displacement and the energy dissipation are considered in the developed program [6]. On the other hand, the shear modulus (G) of reinforced concrete membrane elements subjected to monotonic in-plane shearing stresses typically calculated using the elastic theory was replaced by a simple empirical equation [7]. Rahal presented a simple empirical equation for the calculation of the post-cracking shear modulus, given in the form of the tangent slope of the shear stress-strain curve [7].

In the present work, an improved solution technique is proposed for reinforced concrete membrane element for the case of shear walls subjected to cyclic loading. The proposed solution technique is implemented into a finite element computer program. The finite element computer program is used to study seismic response of a case study with different types of seismic resisting systems which are commonly used in the construction of concrete buildings in Egypt.

2. R/C Plane Stress Element

The formulation of membrane element is based on the modified compression filed theory (MCFT) with the assumption of rotating crack approach. The element stiffness matrix is derived from the flowing integral which will be obtained numerically,

$$[k] = t \int_A [B]^T [D] [B] dA \quad (1)$$

where t is the element thickness, and $[D]$ is the material constitutive matrix based on the current state of element.

In construction of plane stress element stiffness matrix $[k]$, the material stiffness $[D]$ is required to relate stresses $\{\sigma\}$ to strains $\{\varepsilon\}$, that is:

$$\{\sigma\} = [D]\{\varepsilon\} \quad (2)$$

where $\{\sigma\} = \{\sigma_x \ \sigma_y \ \tau_{xy}\}^T$, and $\{\varepsilon\} = \{\varepsilon_x \ \varepsilon_y \ \gamma_{xy}\}^T$.

The stress strain matrix $[D]$ for reinforced concrete membrane element in the x - y coordinate will take the form:

$$[D] = [T]^T [D]_{cl} [T] + [T]^T [D]_{si} [T] \quad [2] \quad (3)$$

where $[D]_{cl}$ is the stress strain matrix for concrete in the local principal stress coordinates, $[D]_{si}$ is the stress strain matrix for reinforcement in the steel local coordinates relative to the x - y coordinates, and $[T]$ is the transformation matrix from the material local coordinates into the x - y global coordinates. Not that $[T]$ will be has different values for both concrete and reinforcement.

2.1 States of Stress-Strain Matrix $[D]$

For linear elastic isotopic material in a plane stress state, the stress strain matrix for concrete $[D]_c$ will take the form:

$$[D]_c = \frac{E_c}{1-\nu^2} \begin{bmatrix} 1 & \nu & 0 \\ \nu & 1 & 0 \\ 0 & 0 & (1-\nu)/2 \end{bmatrix} \quad [2] \quad (4)$$

where E_c is the initial tangent modulus for concrete, and ν is the Poisson's ratio for concrete material in the elastic state.

In the elastic state the stress-strain matrix $[D]_c$ in the local coordinates of principal stresses will be the same in the global coordinates. For nonlinear stress-strain matrix, three Cartesian coordinates, x - y , 1-2, and x_{si} - y_{si} , are defined in reinforced concrete elements, as demonstrated in Figure 1 Coordinate x - y represents the local coordinate of the elements. Coordinate 1-2 defines the principal stress directions of the applied stresses, which have an angle θ_1 with respect to the x -axis. Steel bars can be oriented in different directions in the elements. Coordinate x_{si} - y_{si} shows the direction of the 'ith' group of rebars, where the 'ith' group of rebars are located in the direction of axis x_{si} with an angle θ_{si} to the x -axis.

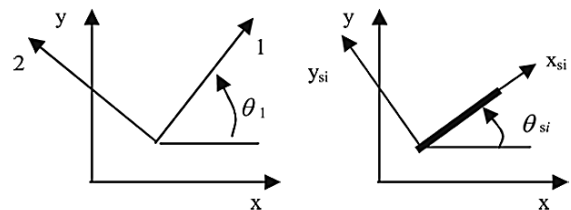


Figure 1: Coordinate System for Reinforced Concrete Element.

If the strains in the x - y direction are $\{\varepsilon_x \ \varepsilon_y \ \gamma_{xy}\}^T$, then the strains in the coordinate system 1-2 will be $\{\varepsilon_1 \ \varepsilon_2 \ \gamma_{12}\}^T$ will be related to the x - y direction strains by the following equation:

$$\begin{Bmatrix} \varepsilon_1 \\ \varepsilon_2 \\ \gamma_{12} \end{Bmatrix} = [T(\theta_1)] \begin{Bmatrix} \varepsilon_x \\ \varepsilon_y \\ \gamma_{xy} \end{Bmatrix} \quad (5)$$

Considering $c = \cos(\theta_1)$ and $s = \sin(\theta_1)$, then the transformation matrix $[T(\theta_1)]$ will be calculated from the following equation

$$[T(\theta_1)] = \begin{bmatrix} c^2 & s^2 & cs \\ s^2 & c^2 & -cs \\ -2cs & 2cs & c^2 - s^2 \end{bmatrix} \quad (6)$$

$$\theta_1 = \tan^{-1} \left(\frac{0.5\gamma_{xy}}{(\varepsilon_x - \varepsilon_{c2})} \right) \quad \varepsilon_x \neq \varepsilon_{c2} \quad (7)$$

$$\theta_1 = 0 \quad \varepsilon_x = \varepsilon_{c2}$$

For cracked concrete, having strains in the principal directions, the corresponding tangent stiffness modulus for each direction is calculated according to the chosen material model described in the previous subtitles. In the current study the Poisson's ratios are neglected after cracking. The local 1-2 concrete stress-strain matrix $[D]_{cl}$ will be:

$$[D]_{cl} = \begin{bmatrix} E_{c1} & 0 & 0 \\ 0 & E_{c2} & 0 \\ 0 & 0 & G_{12} \end{bmatrix} \quad (8)$$

where G_{12} is the tangent shear modulus calculated from,

$$G_{12} = \frac{\sigma_{1c} - \sigma_{2c}}{2(\varepsilon_1 - \varepsilon_2)} \quad [10] \quad (9)$$

where σ_{1c} and σ_{2c} are the concrete stresses in 1- and 2-direction respectively and their corresponding strains ε_1 and ε_2 , respectively.

If two perpendicular reinforcements are used in l-t direction reinforcement are aligned with an angle of θ_{si} from the x-y direction, the strains $\{\varepsilon_x \ \varepsilon_y \ \gamma_{xy}\}^T$ from x-y coordinate will be transformed to the l-t coordinate system using:

$$\begin{Bmatrix} \varepsilon_l \\ \varepsilon_t \\ \gamma_{lt} \end{Bmatrix} = [T(\theta_{si})] \begin{Bmatrix} \varepsilon_x \\ \varepsilon_y \\ \gamma_{xy} \end{Bmatrix} \quad (10)$$

Considering that the steel mesh will not resist any shear stresses; then the stress-strain matrix $[D]_{sl}$ in coordinate l-t will be calculated from:

$$[D]_{sl} = \begin{bmatrix} \rho_l E_{sl} & 0 & 0 \\ 0 & \rho_t E_{st} & 0 \\ 0 & 0 & 0 \end{bmatrix} \quad (11)$$

where E_{sl} and E_{st} are the tangent stiffness for reinforcement in l- and t-directions, respectively.

Finally the composite reinforced concrete stress-strain matrix is transformed into x-y direction using:

$$[D] = [T(\theta_1)]^T [D]_{cl} [T(\theta_1)] + [T(\theta_{si})]^T [D]_{sl} [T(\theta_{si})] \quad (12)$$

2.2 Crack Angle Algorithm

According to the assumption of smeared rotating crack, the crack direction is changed continuously during nonlinear analysis according to the principal strains directions. Each direction has its nonlinear history parameters specially when dealing with cyclic loading. These nonlinear parameters (i.e. current strain, maximum/minimum strains and stresses, plastic strains, etc...) must be recorded for each principal direction. For the case of reversed loading, the principal tensile direction was the principal compression one earlier, but the nonlinear parameters recorded in the previous step must be switched between these directions if the angle between the current and the previous directions is about 90 degrees.

In order to capture this process automatically during nonlinear analysis, an algorithm is proposed as follows:

- Check is $|(\theta_{lprev} - \theta_l)|$ greater than or equal to 45° and $|(\theta_{lprev} - \theta_l)|$ less than or equal to 135° .
- If the previously stated condition is satisfied, then keep both recorded nonlinear data in the same directions and set $\theta_{lprev} = \theta_l$.
- Otherwise, switch the nonlinear data between principle directions and set θ_{lprev} equal to $\theta_l - 90^\circ$ if θ_l is greater than θ_{lprev} and set θ_{lprev} equal $\theta_l + 90^\circ$ otherwise.

The above procedure allows switching the nonlinear parameters automatically between principle strain directions. Implementation of crack angle algorithm in the element resistance nodal forces process of the reinforced concrete plane stress element is illustrated in Figures 2 and 3.

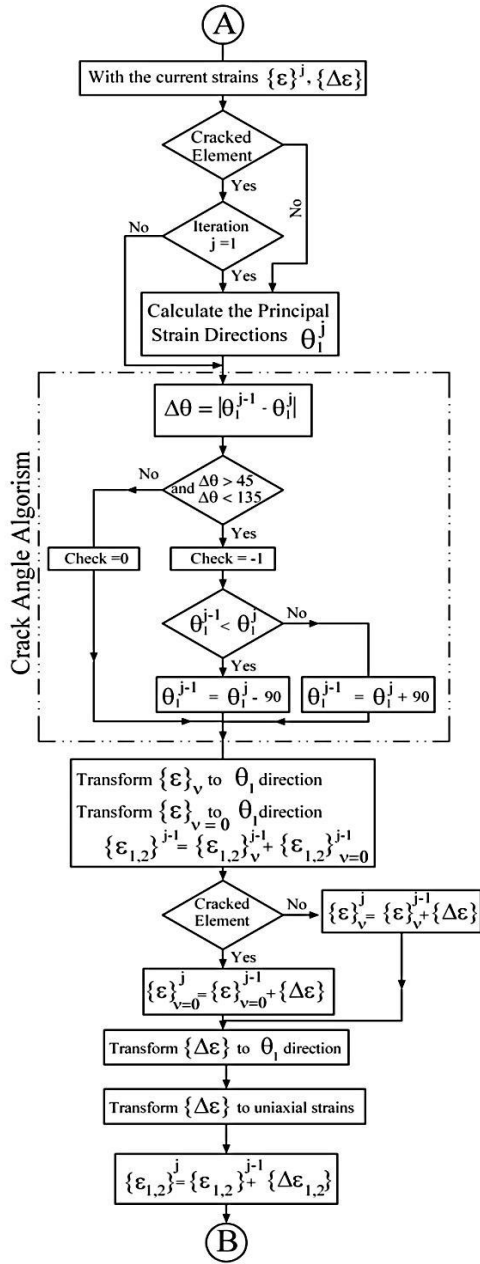


Figure 2: Crack angle algorithm implementation and principle strains calculation procedure.

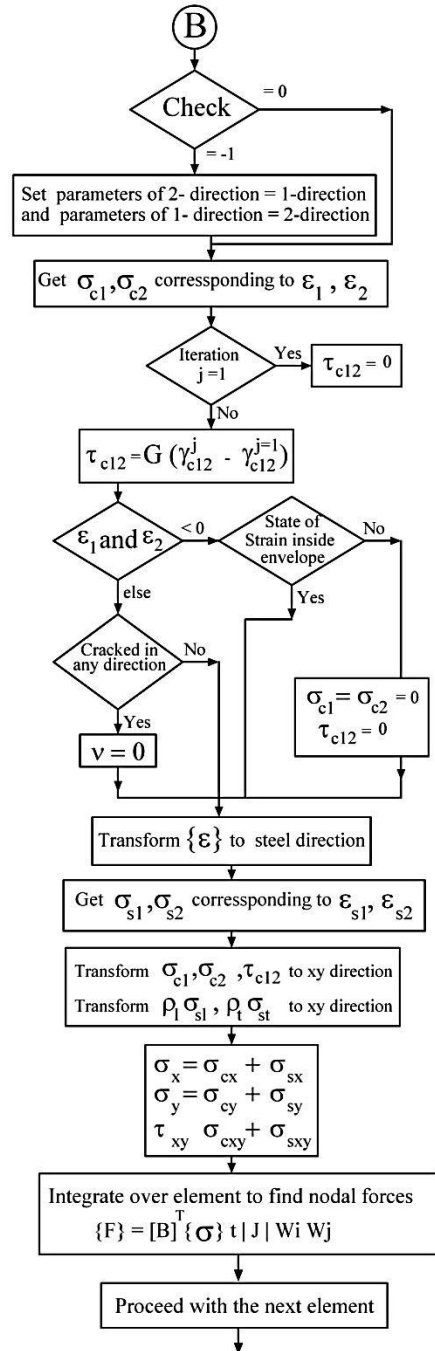


Figure 3: Calculation of plane stress element equivalent resistance nodal forces.

3. Material Modeling

Different types of uniaxial stress strain curves are adopted in the finite element program for both concrete and reinforcing steel.

3.1 Concrete Envelope Curves

3.1.1 Compression envelopes

The stress strain curve for concrete in compression by Kent [8] for unconfined and confined concrete is

used in the present study. The model generalized Hognestad equation to more completely describe the post-peak stress-strain behavior [9]. For unconfined concrete the envelope is defined by:

$$f_{ci} = f'_c \left\{ 2 \left(\frac{\varepsilon_{ci}}{\varepsilon_{co}} \right) - \left(\frac{\varepsilon_{ci}}{\varepsilon_{co}} \right)^2 \right\}, \quad \varepsilon_{ci} \leq 0.002 \quad (13)$$

$$f_{ci} = f'_c [1 - z(\varepsilon_{ci} - \varepsilon_{co})] \quad \varepsilon_{ci} > 0.002 \quad (14)$$

$$z = \frac{0.5}{\varepsilon_{50u} - \varepsilon_{co}} \quad (15)$$

$$\varepsilon_{50u} = \frac{3 + 0.29f'_c}{145f'_c - 1000}, \quad f'_c \text{ in [MPa]} \quad (16)$$

For confined concrete, Confinement only affected the slope of the post-peak branch and is given by

$$f_{ci} = f'_c [1 - z(\varepsilon_{ci} - \varepsilon_{co})] \quad (17)$$

$$z = \frac{0.5}{\varepsilon_{50h} + \varepsilon_{50u} - \varepsilon_{co}} \quad (18)$$

$$\varepsilon_{50h} = \varepsilon_{50c} - \varepsilon_{50u} = \frac{3}{4} p'' \sqrt{\frac{b''}{s}} \quad (19)$$

$$\varepsilon_{50u} = \frac{3 + 0.29f'_c}{145f'_c - 1000}, \quad f'_c \text{ in [MPa]}$$

where ε_{50c} and ε_{50u} are the strains corresponding to the stress equal to 50% of the maximum concrete strength for confined and unconfined concrete, respectively. $\frac{b''}{s}$ is the ratio between the width of the concrete core and the center to center spacing of hoops, p'' is the volumetric ratio of confining hoops to volume of concrete core measured to the outside of the perimeter hoops and is expressed as:

$$p'' = \frac{2(b'' + d'')As''}{b''d''s} \quad (20)$$

where b'' and d'' are the width and depth of the confined core respectively, As'' is the cross-sectional area of the hoop bar and s is the center to center spacing of the hoops.

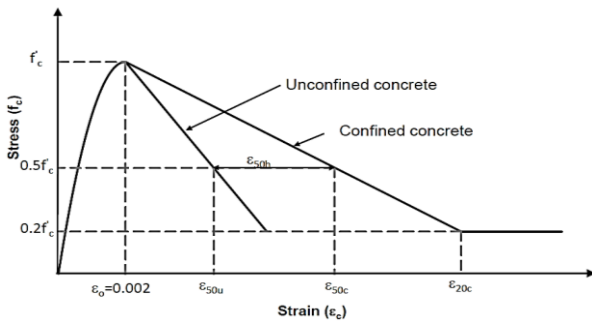


Figure 4: Stress-strain model for confined and unconfined concrete [8].

3.1.2 Tension envelopes

In the present paper linear and the exponential softening patterns presented by He [10] are used, Figure 5. The exponential function for concrete response in tension after cracking involving limiting value of ultimate tensile strain based on crack failure energy.

$$f_t = \begin{cases} E_c \varepsilon & \varepsilon \leq \varepsilon_{cr} \\ f_{cr} \exp\left(-\frac{\varepsilon - \varepsilon_{cr}}{\varepsilon_{tu} - \varepsilon_{cr}}\right) & \varepsilon_{cr} < \varepsilon < \varepsilon_{tu} \\ 0 & \varepsilon > \varepsilon_{tu} \end{cases} \quad (21)$$

where, ε_{tu} is the ultimate tensile strain which is determined from the tensile fracture energy G_f and determined from

$$\varepsilon_{tu} = \frac{G_f}{hf_{cr}} + 0.5\varepsilon_{cr} \quad (22)$$

where h is the crack band width and related to the area of the finite element, A , by the following relation

$$h = \alpha\sqrt{A} \quad (23)$$

where $\alpha = \sqrt{2}$ is factor with a suggested value [10].

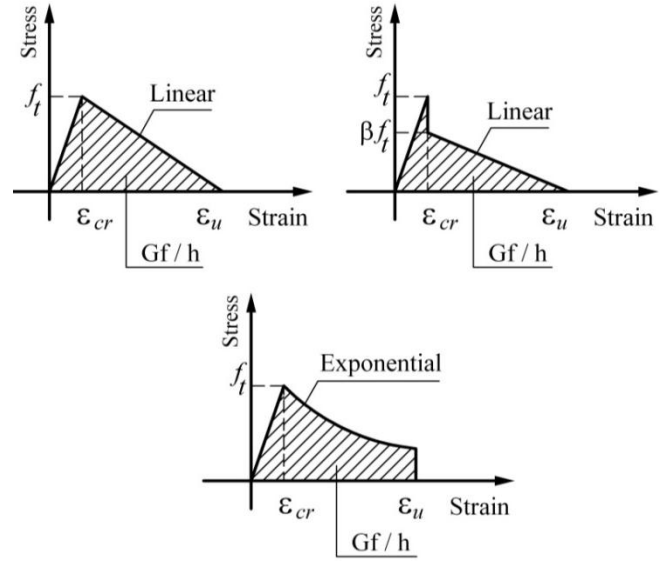


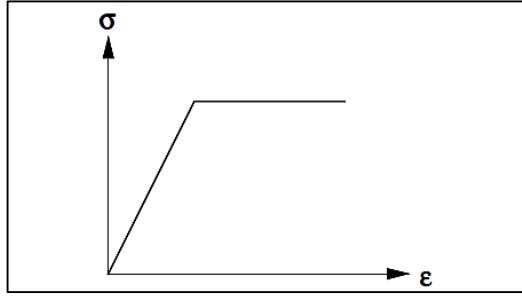
Figure 5: Common types of tension stiffening models.

3.2 Reinforcing Steel Envelope Curves

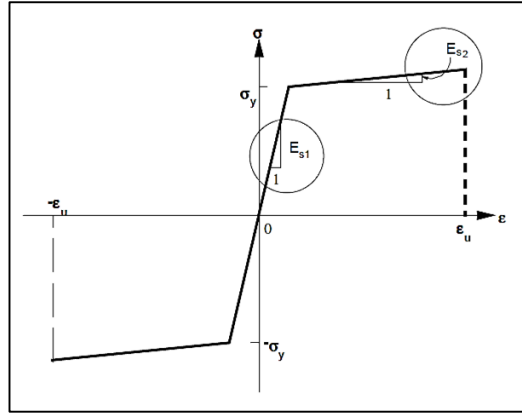
The first idealization neglects the strength increase due to strain hardening and the reinforcing steel is modeled as a linear, perfectly plastic material, as shown in (Figure 6-a). More accurate idealizations which account for the strain hardening effect are required, as shown in Figure 6-b. The parameters of these models are the stress and strain at the onset of yielding (f_y, ε_y), the strain at the onset of strain hardening and the stress and strain at ultimate (f_{max}, ε_u). These parameters can be derived from experimentally obtained stress-strain relations.

$$f_s = \begin{cases} E_s \varepsilon & \varepsilon \leq \varepsilon_y \\ f_y + bE_s(\varepsilon - \varepsilon_y) & \varepsilon_y < \varepsilon \leq \varepsilon_u \\ 0 & \varepsilon > \varepsilon_u \end{cases} \quad (24)$$

where E_s is the initial tangent modulus for steel material, f_y is the yield strength for reinforcement steel, b is the hardening tangent modulus ratio, and ε_u is the ultimate strain of reinforcement steel.



(a) elastic-perfect plastic model



(b) elastoplastic with strain hardening ratio

Figure 6: Idealized steel stress-strain relation

3.3 Concrete Hysteretic Model

Different models for concrete hysteretic behavior were presented and discussed in the literature. In the present research some simplifications for the model presented by He were made [10]. A linear loading/reloading paths from tension or compression domains were assumed, Figure 7-a. The plastic compressive and tensile strains are calculated from:

$$\varepsilon_c^{pl} = \varepsilon_c^{min} - \frac{20}{7} \left[1 - \exp\left(-0.35 \frac{\varepsilon_c^{min}}{\varepsilon_c^o}\right) \right] \varepsilon_c^o \quad (25)$$

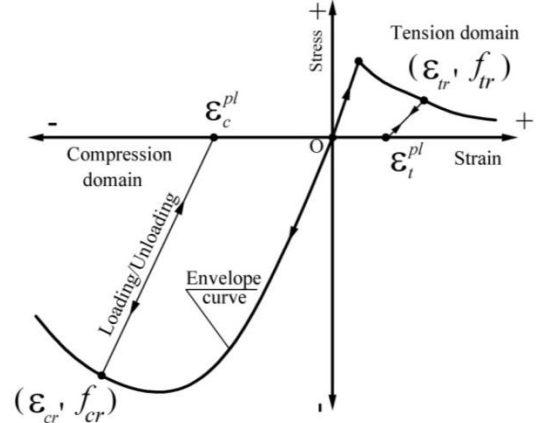
$$\varepsilon_t^{pl} = \begin{cases} 0 & \varepsilon_t \leq \varepsilon_t^{cr} \\ 0.9\varepsilon_t^{max} - 0.8\varepsilon_t^{cr} & \varepsilon_t < \varepsilon_t^{cr} \end{cases} \quad (26)$$

where ε_c^{min} and ε_c^o are the maximum experienced compressive strain and strain corresponding to peak stress on the compression envelope curve. ε_t^{max} and ε_t^{cr} are the maximum experienced tensile strain and cracking strain of concrete. Under reversed cyclic loading, concrete may repeatedly experience crack closing and reopening. Hence, we need to define a path

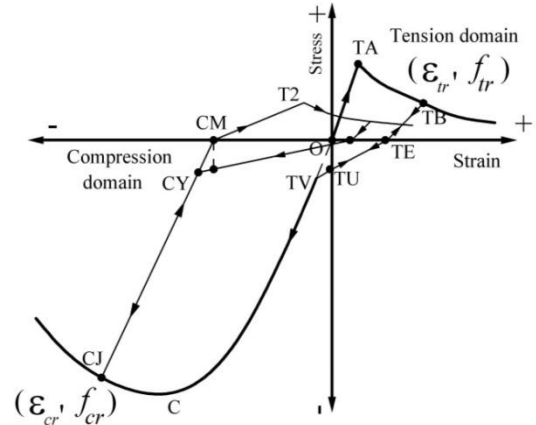
for the process. The stress required to cause crack close can be expressed as follows:

$$\sigma_{crack}^{close} = -f_t \left(0.05 + \frac{0.03\varepsilon_t^{max}}{\varepsilon_t^{cr}} \right) \quad (27)$$

The path of the crack closing is illustrated by a straight line that connects points **TE** and **TU**, as shown in Figure 7-b.



(a) Linear unloading/reloading paths



(b) transition from compression to tension

Figure 7: Concrete hysteretic behavior modified from He et al. [10]

3.4 Reinforcing Steel Hysteretic Model

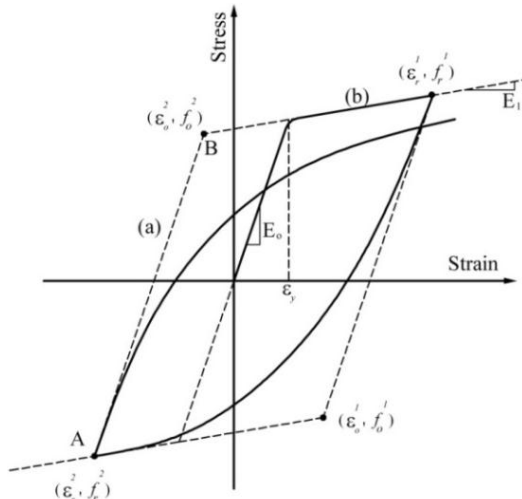
Previous research shows that the Menegotto-Pinto equation represents well the unloading and reloading response of reinforcing steel subjected to cyclic loading. The model as presented in Menegotto [11] is used in the present work as follows:

$$f^* = b \cdot \varepsilon^* + \frac{(1-b) \cdot \varepsilon^*}{(1 + \varepsilon^{*R})^{1/R}} \quad (28)$$

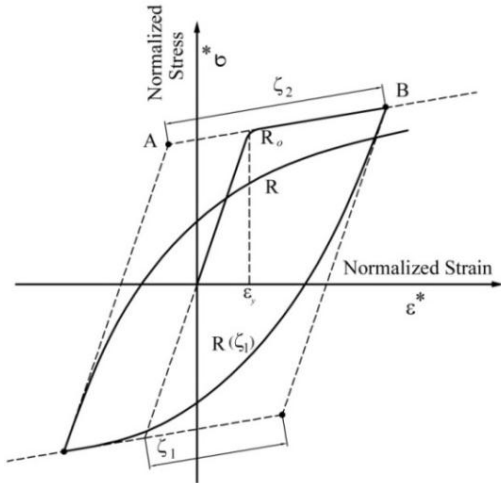
$$\varepsilon^* = \frac{\varepsilon - \varepsilon_r}{\varepsilon_o - \varepsilon_r} \quad (29)$$

$$f^* = \frac{f - f_r}{f_o - f_r} \quad (30)$$

Eq. (28) represents a curved transition from a straight line asymptote with slope E_0 to another asymptote with slope E_1 (lines (a) and (b), respectively, in Figure 8-a), and ε_o are the stress and strain at the point where the two asymptotes of the branch under consideration meet (point B in Figure 8-a); similarly, σ_r and ε_r are the stress and strain at the point where the last strain reversal with stress of equal sign took place (point A in Figure 8-a); b is the strain hardening ratio, that is the ratio between slope E_1 and E_0 and R is a parameter that influences the shape of the transition curve and allows a good representation of the Bauschinger effect.



(a) transition from linear-elastic to plastic after yield



(b) definition of parameter "R"

Figure 8: Menegotto-Pinto steel model [11].

As indicated in Figure 8-a, $(\varepsilon_o, \sigma_o)$ and $(\varepsilon_r, \sigma_r)$ are updated after each strain reversal. R is considered dependent on the strain difference between the current asymptote intersection point (point A in Figure 8-b) and the previous load reversal point with maximum or minimum strain depending on whether the

corresponding steel stress is positive or negative (point B in Figure 8-b). The expression for R takes the form

$$R(\xi) = R_o - \frac{a_1 \xi}{a_2 + \xi} \quad [13] \quad (31)$$

where ξ is updated following a strain reversal. R_o is the value of the parameter R during first loading and a_1, a_2 are experimentally determined parameters to be defined together with R_o . The definition of ξ remains valid in case that reloading occurs after partial unloading and calculated from

$$\xi = \begin{cases} \frac{\varepsilon_{st}^{\max} - \varepsilon_o}{\varepsilon_{sy}} & d\varepsilon > 0 \\ \frac{\varepsilon_{st}^{\min} - \varepsilon_o}{\varepsilon_{sy}} & d\varepsilon < 0 \end{cases} \quad (32)$$

In the present research the parameter values are taken as follows: $R_o = 20, a_1 = 18.5, a_2 = 0.15$.

4. Model Verification

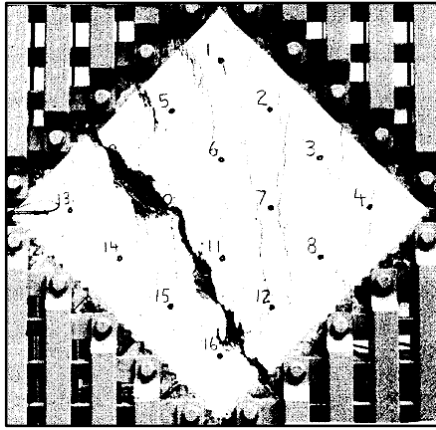
The reinforced concrete plane stress element used in the present work is based on modified compression field theory MCFT with smeared rotating crack approach. Cracking of element is allowed at four integration points. In order to verify the stability and accuracy of the nonlinear implementation, a group of comparisons with experimental results and other published studies is performed.

4.1 Monotonically Loaded Panels

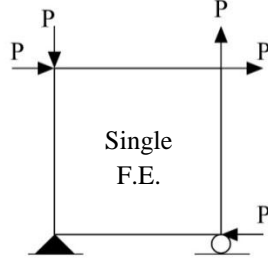
In the experimental work conducted at university of Toronto "Toronto test program" the approach adopted was to subject simple reinforced concrete panel elements to uniformly applied, well –controlled edge loads representing general conditions of in-plane stress using the panel element tester which is capable of loading (890*890*70) mm test specimens under any combination of in-plane stress. Typical panel test and finite element idealization are shown in Figure 7. The original test program involved the 30 panel elements (PV-series specimens) reported by Vecchio and Collins [1]. These panels were orthotropically reinforced and subjected to increasing loads. The following discussion compares the results of the available data for panels PV10 (pure shear) and PV23 (combined shear and axial stresses). Material properties and loading conditions for PV10 and PV23 are summarized in Table 1 while stress-strain relationships are summarized in Table 2.

A single reinforced concrete plane stress element is used to model the panels with four integration points. The loading conditions are idealized to produce the

same applied stresses. The loading configuration for the case of pure shear is shown in Figure 9(b), whereas for the case of biaxial compression with shear stress within the given ratio in Table 1 is shown in Figure 10.



(a) Typical panel under test



(b) Idealized finite element model for direct shear using single element

Figure 9: Tested panels by Vecchio [1] and finite element idealization

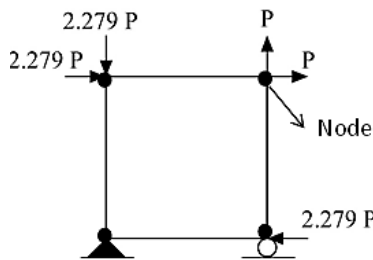


Figure 10: Finite element model and loading conditions for panel PV23.

Since, the element material properties and stress conditions are uniform throughout the element, modeling of panels with single element is sufficient. In the current analysis, linear softening model for concrete in cracking was assumed with tensile strength of 1.6 and 2.2 MPa for specimens PV10 and PV23 respectively. The compressive strength of concrete subjected to transverse tensile stress is reduced [1]. Good correlation between the predicted and experimental results was observed as illustrated in Figures 9 and 10. On the other hand, the predicted

failure modes and shear stress versus shear strain response are evaluated accurately.

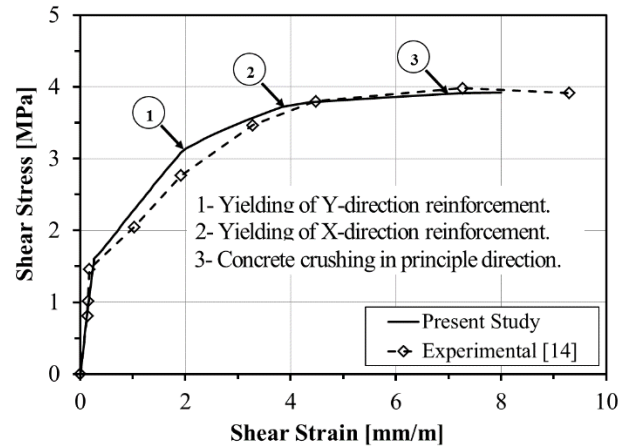


Figure 11: Correlation between predicted and experimental results for specimen PV10.

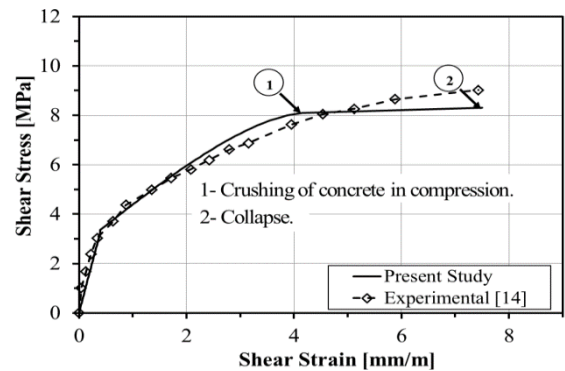


Figure 12: Correlation between predicted and experimental results for specimen PV23.

Table 1: Concrete material properties and loading conditions for specimens PV10 and PV23 [1]

Panel	Concrete [MPa]	Reinforcement			Loading Ratio		
		X	Y	f_y [MPa]	τ	σ_x	σ_y
	f_c'	ρ_x %	ρ_y %				
PV10	14.5	1.79	1	276	1	0	0
PV23	20.5	1.79	1.79	518	1	-0.39	-0.39

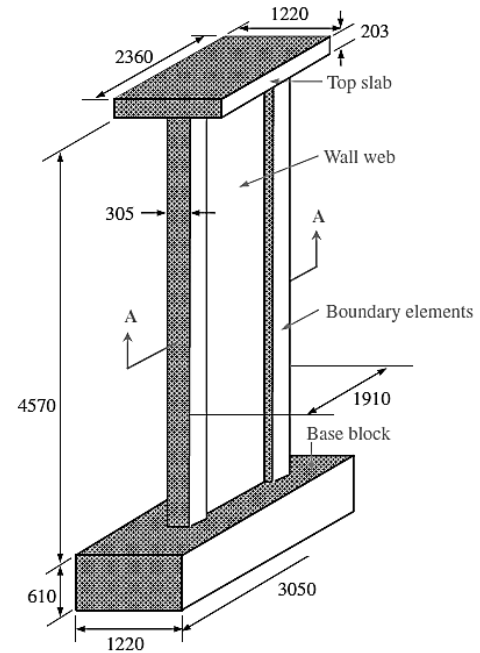
Table 2: Material properties and stress strain curves for specimens PV10 and PV23.

Material	Material Modeling
Concrete	Compression: Kent and Park model [8], $E_c = 18$ GPa for $f_c' = 14.5$ and $E_c = 22$ GPa for $f_c' = 20.5$ Tension: Linear softening $\epsilon_{tu} = 0.001$, $f_t = 1.6$ MPa for PV10 and $f_t = 2.2$ MPa for PV23
Reinf.	Bilinear with 2% strain hardening ratio.

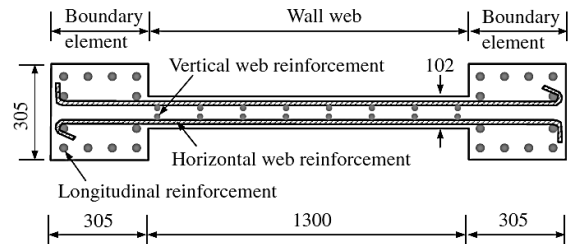
4.2 Cyclically Loaded Walls

To verify the cyclic behavior of implemented reinforced concrete plane stress element for cyclic loading for structural scale, the shear wall B2 tested by Oesterle at the Portland Cement Association, was examined [12]. The barbell-shaped wall B2 shown in Figure 13 was a one-third scale representation of a five-story wall, and was framed with the base block, the stiff top slab, the wall web, and boundary elements. The wall web was 4570 mm high x 1910 mm long x 102 mm thick, and was reinforced with 0.63% and 0.29% reinforcing ratios in the horizontal and vertical directions, respectively. The elements boundary had the dimensions 4570 mm high x 305 mm long x 305 mm thick, and had a vertical reinforcing ratio of 3.67%. The details of the geometry and the layout of the reinforcement are given in Figure 14.

The material properties for the specimen are shown in Table 3. Stress strain relationships and hysteric models are summarized in Table 4. A lateral load was applied at the top of the specimen through the stiff top slab. The specimen was subjected to a cyclic displacement loading history in the experimental program; while in the present analysis is subjected to cyclic force history of constant maximum force of 743 kN. The shear wall B2 was modeled by a 254-element mesh with four-node plane stress quadrilateral elements, as shown in Figure 14 the mesh was divided into three zones to represent the top slab, the wall web, and the boundary elements. The thickness of these three zones was varied to reflect changes in their cross-sectional geometry. The base block was omitted from the analysis, and the nodes at the base of the wall were therefore fully fixed against horizontal and vertical translations. The top slab was assumed to be rigid to distribute the load to the entire structural cross-section. The loading history was imposed at the upper nodes of the top slab (Figure 14). The steel reinforcing bars were modeled as smeared within concrete elements, and a perfect bond between the concrete and the steel was assumed. The material properties and the reinforcing ratios as used in the analysis are listed in Tables 2 and 3. In the numerical analyses, the loading step was set to 10kN with total number of steps of 600 steps. The tolerance for divergence was 5%.



(a) Nominal dimensions of test specimen (all dimensions in mm)



(b) Reinforcement of section A-A (dim. in mm)

Figure 13: Details of shear wall B2 [12].

Table 3: Material properties for shear wall B2

Material	Properties	Wall Web	Boundary Elements
Concrete	Young's modulus E_c (GPa)	32.7	32.70
	Poisson's ratio ν	0.20	0.20
	Compr. Strength f_c' (MPa)	53.70	53.70
	Tensile Strength f_t (MPa)	4.29	4.29
Horizontal reinf.	Young's modulus E_s (MPa)	200	200
	Strain hardening ratio (%)	2	2
	Yield Strength f_y (MPa)	532.4	532.4
	Reinforcing ratio ρ (%)	0.63	0.63
Vertical reinf.	Young's modulus E_s (MPa)	200	200
	Strain hardening ratio (%)	2	2
	Yield Strength f_y (MPa)	532.4	532.4
	Reinforcing ratio ρ (%)	0.29	3.67

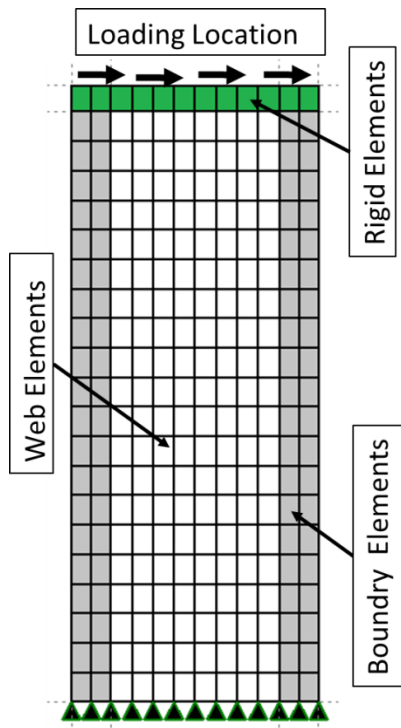


Figure 14: Finite element model for shear wall with elements at boundaries.

Table 4: Stress strain relationships Oesterle wall [12].

Material	Material Modeling
Concrete	Compression: Kent and Park model [8] Tension: Linear softening $\epsilon_{tu} = 0.0015$ Hysteretic Model: Simplified He et al. [10] (subsection 3.3)
Reinf.	Bilinear with 2.0% strain hardening ratio. Hysteretic Model: Menegotto-Pinto [11] (subsection 3.4)

The calculated and measured applied load-top deflection curves are shown in Figure 15. Generally, the calculated response agrees with the experimental results and the predicted response by He et al. [10]. The calculated lateral resistance of the wall is 743 kN, which gives a satisfactory prediction of the measured resistance of 692 kN. The calculated lateral stiffness of the wall degrades progressively as the number of load cycles increases, in accordance with the observed experimental response.

Figure 16 illustrates the predicted crack patterns, which are denoted by the crack strains in the direction normal to cracking, at the first +743 kN and -743 kN loading cycles. The calculated crack patterns are characterized by the diagonal cracks crisscrossing the wall web and the diagonal cracks near the base of the wall realigning to be more horizontal, which agree well with the experimental observations reported by Oesterle [12]. Figure 17 shows the calculated principal compressive strain distribution in the wall at the first

± 743 kN loading cycles. The analysis predicts large tensile strain at the low portion of the wall on the side and large compressive strain near the base of the wall. This results in a relatively localized zone of high compressive stresses near the interface of the wall web and the boundary elements. Thus, the calculated failure mode occurs due to the crushing of concrete at the compressive side near the base of the wall. Figure 18 shows the calculated principal tensile strain distribution in the wall at the first ± 743 kN loading cycles. The results show high tensile strains localized perpendicular to the major shear cracks inclined nearly to 45 degrees and starting from wall base section. Note that the hysteretic loops from the experiment are more pinched than the calculated loops (see Figure 15). This attributes to the shear slip along the crack surfaces, which results in a reduction of the wall's capacity for energy dissipation. To accurately predict the structural behavior under such a situation, the bond-slip model of the reinforcement needs to be taken into account.

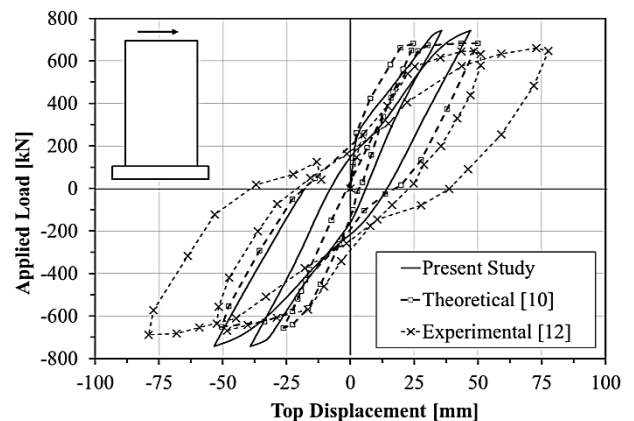


Figure 15: Correlation between the predicted and experimental top displacement.

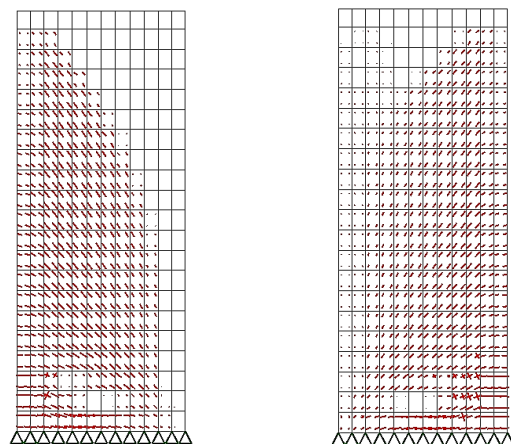
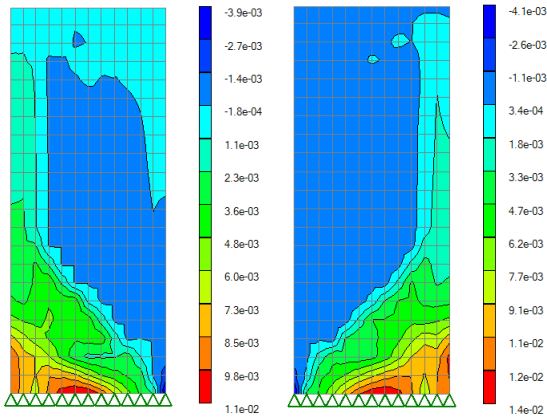
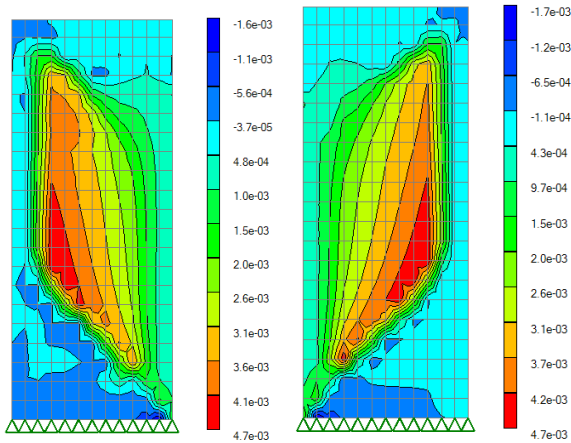


Figure 16: Predicted crack pattern in shear wall B2.



at first +743 kN load cycle at first -743 kN load cycle
Figure 17: Principal compressive strains for shear wall B2.



at first +743 kN load cycle at first -743 kN load cycle
Figure 18: Principal tensile strains for shear wall B2.

5. Behavior of Seismic Resisting Systems

The delegate 2 by 3 bays reinforced concrete building is used for the purpose of parametric study. The plan dimensions were 12x15 m with ground floor height of 4 m and 3 m for repeated typical floors. The floor slabs are divided into two categories, flat slab system and slab-beam system, (see Figures 17, 18, and Table 5). Two common types of lateral load resisting systems which are commonly used in Port-Said area were examined. In these systems the lateral load is resisted by columns or by dual system, consists of frame and shear walls. The tested buildings were 6, 9, and 12 stories for low, medium, and high rise, respectively. The building location is classified in zone (3) according to ECP-201 [13]. The building vertical elements were designed under the effect of vertical loads and earthquake loading according to Egyptian Code of Practice [14] and Egyptian Code for Loads [13].

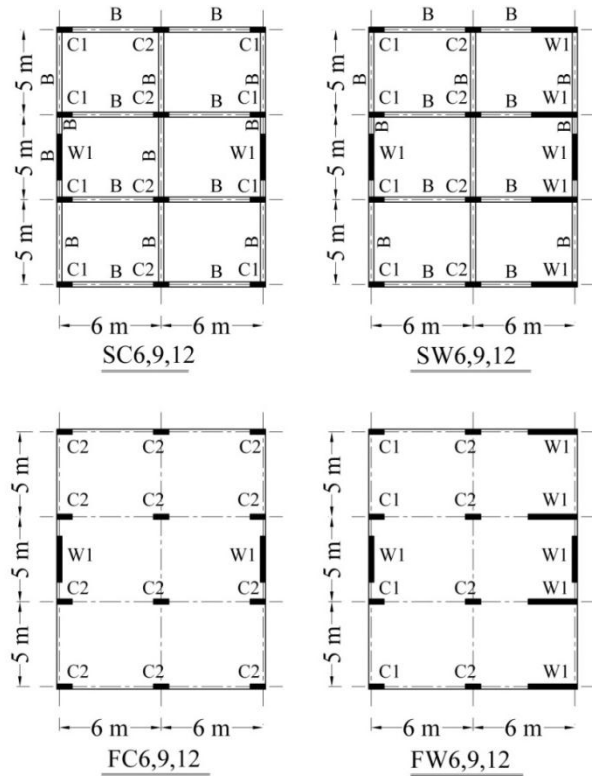
Systems Designation Rule

Floor Type	Vertical Elements	No. of Stories
Slab-Beam[S]	Columns only [C]	6, 9, and 12
Flat Slab [F]	Columns and Walls [W]	

Example: SW12

12 stories building with slab-beam floor and the vertical resisting elements composed from columns and shear walls.

(a) Systems designation rule



(b) Typical floor structural plan for different systems

Figure 19: Configuration of study systems.

Table 5: Cross-section assignments for different buildings systems.

Building Layout	Number of Stories	Floor System	C1-Detail	C2-Detail	W1-Detail	Beams
FC6	6	Flat-Slab	C	C	---	G
FC9	9	Flat-Slab	D	D	---	G
FC12	12	Flat-Slab	E	E	---	G
FW6	6	Flat-Slab	A	C	W1	G
FW9	9	Flat-Slab	B	D	W1	G
FW12	12	Flat-Slab	C	E	W1	G
SC6	6	Slab-Beam	A	C	---	B
SC9	9	Slab-Beam	B	D	---	B
SC12	12	Slab-Beam	C	E	---	B
SW6	6	Slab-Beam	A	C	W1	B
SW9	9	Slab-Beam	B	D	W1	B
SW12	12	Slab-Beam	C	E	W1	B

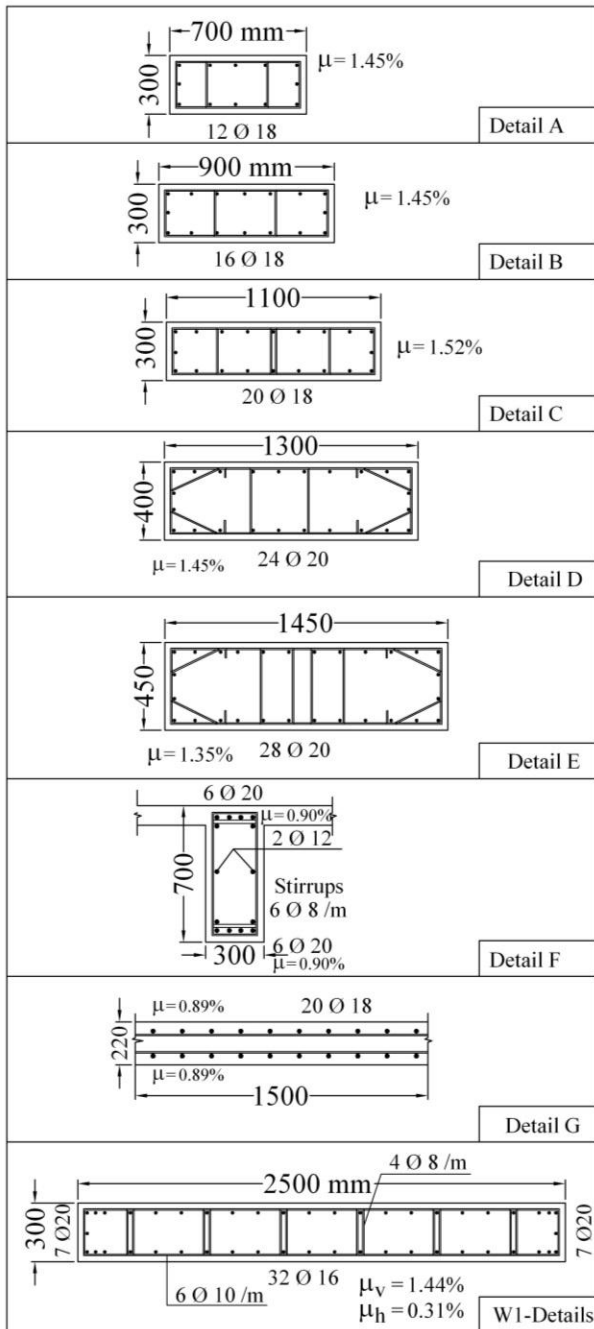


Figure 20: Cross section details for columns, walls and beams

The concrete floor dimensions were chosen to ensure that the average floor weight is almost the same for both flat and solid slab systems. The super imposed dead load was 4 kN/m², which include the average weight of brick walls and flooring covering. The live load was chosen 2 kN/m² for residential use. The material of construction was: Concrete characteristic strength $f_{cu}=30$ MPa, main steel yield strength $f_y = 360$ MPa with ultimate strength of $f_u =520$ MPa, and stirrups material for both beams and columns has yield

strength of 240 MPa. The material modeling is summarized in Table 6.

Table 6: Material properties and stress strain curves for the case study.

Material	Material Modeling
Concrete	Compression: Kent and Park model [8], $E_c = 24$ GPa, $f_c' = f_{co} = 24$ MPa, Tension: Linear softening $\epsilon_{tu} = 0.001$, $f_t = 2.5$ MPa Hysteretic Model: Simplified He et al [10] (subsection 3.3)
Reinf.	Bilinear with 3.0% strain hardening ratio. $f_y = 360$ MPa, $E_s = 200$ GPa Hysteretic Model: Menegotto-Pinto [11] (subsection 3.4)

5.1 Structural Modeling and Loading Configurations

For buildings of symmetric plans, where the stiffness of each horizontal resisting system is the same, selecting of a 2D system to represent the whole behavior of the structure is acceptable. For floors with projected beams, the stiffness of slabs could be ignored and used only to ensure equal horizontal displacements of all plane frames due to their high in-plane rigidity. For flat slab systems, six times slab thickness plus column width in addition to in-plane rigidity could be used according to ECP-203 [14]. The columns and beams were modeled using flexibility based beam-column element while shear walls were modeled using the improved plane stress reinforced concrete element. For both floor types (i.e. with/without projected beams), a schematic load configuration is shown in Figure 21 and Table 7. For flat system, the distributed load is calculated on the basis of effective slab width which resists lateral loads according ECP-201 [13], while the remaining part of floor loads was lumped at the column locations. The concentrated loads also include the effect of masonry walls and beams reaction if any in the out of plane direction.

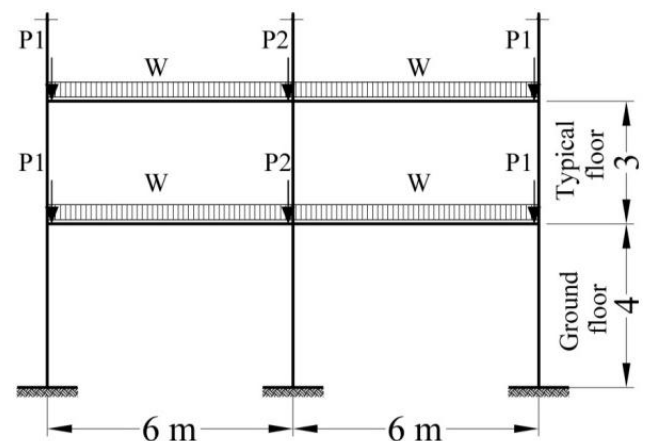


Figure 21: Elevation of 2D plane systems showing loading configuration under vertical loads.

Table 7: Calculated loading values for 2D plane systems.

Floor Systems	P1 [kN]		P2 [kN]		W [kN/m]	
	Dead Load	Live Load	Dead Load	Live Load	Dead Load	Live Load
Slab-Beam	60	10	147	30	28	6
Flat-Slab	77	16.3	159.5	33.7	21.4	4.5

6. Nonlinear Static Analysis Results

The nonlinear static analysis for triangular load pattern representing seismic equivalent static effect is performed. The monotonic lateral load is increased in conjunction with sustainable vertical loads until the system is collapsed. The following normalized parameters are predicted, Figure 22.

- Story lateral drift $[\delta]$ divided by story height $[z]$ measured from foundation level.
- Interstory lateral drift $[\Delta]$ divided by floor height $[h]$.

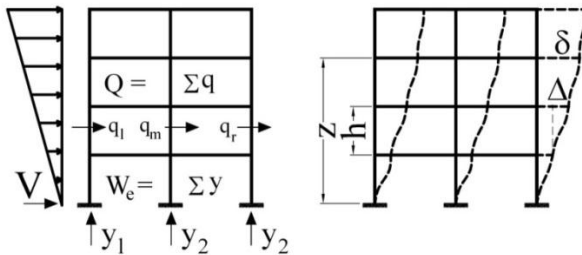


Figure 22: Definition of study output parameters.

6.1 Top Story Lateral Drift Ratio

Top story lateral drift ratio (δ/z) versus base shear ratio (V/W_e) for different systems is shown in Figures 23 to 26. Due to its low floor stiffness compared to slab-beam systems, flat slab systems showed lower stiffness. Moreover, the response of flat slab systems tends to have flat plateau near collapse load due to forming of plastic hinges at sections near column faces. On the other hand, the failure mechanism for slab beam systems is started by yielding of beams/columns reinforcement localized at lower floors and then continued to the upper floors followed by crushing of concrete at column sections at foundation level.

6.2 Failure Base Shear Ratio

The collapse base shear and the base shear ratio (V/W_e) corresponding to top story lateral drift ratios $(\delta/z) = 0.2\%$ are listed in . The (V/W_e) ratio versus top story lateral drift ratio (δ/z) for different building

heights are shown in Figures 27 to 29. As expected, the flat slab systems without shear walls showed lower collapse base shear ratio than other systems. In addition, for systems without shear walls, the ratio between base shear ratio corresponding to 0.2% code limitation for top story lateral drift ratio for flat slab systems (FC) was about twice its value for solid slab systems (SC) indicating more ductility for (FC) systems. Moreover, the base shear ratio (V/W_e) decreases with the increase of building height and it is increased with system stiffness.

6.3 Interstory Drift Ratio

The interstory lateral drift ratio (Δ/h) is the value that indicates the amount of story lateral distortion which affects the non-structural components and may cause its damage. Therefore design codes limit this value to a specified ratio ensuring minimum damage of story nonstructural components. The Egyptian code limits this ratio to 1/200 of floor height [13]. The vertical distributions of interstory lateral drift ratio (Δ/h) for the examined structural systems prior to collapse are shown in Figures 30 to 33. In general, the (Δ/h) ratio increases gradually from foundation level reaching its maximum value at a certain floor. After that the interstory lateral drift ratio continues vertically in a constant pattern in for flat slab systems (FC, FW) or decreases gradually in slab-beam systems (SC, SW). For SC and SW systems, the critical story which has the maximum value of (Δ/h) is located at about one third building height, while in (FC) and (FW) systems; it is located at about one half of the building height. It was found that the rate of decrease of interstory drift for systems without shear walls is higher than systems with shear walls especially for slab-beam systems.

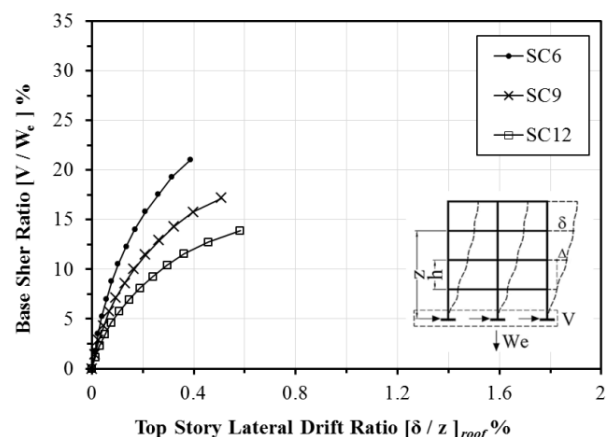


Figure 23: Base shear versus top story lateral drift ratios for SC systems.

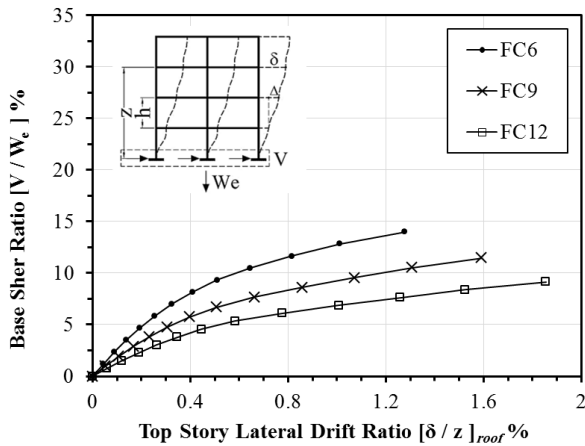


Figure 24: Base shear versus top story lateral drift ratios for FC systems.

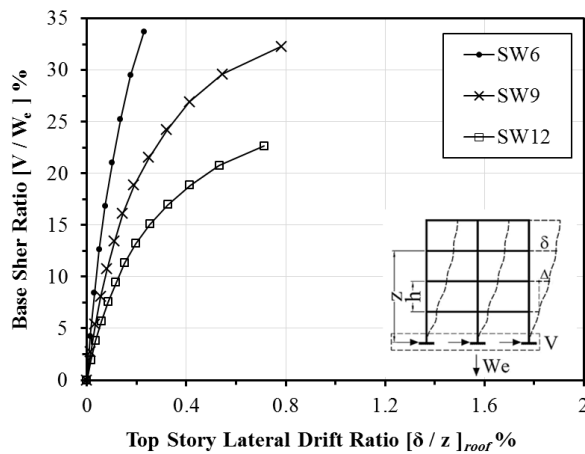


Figure 25: Base shear versus top story lateral drift ratios for SW systems.

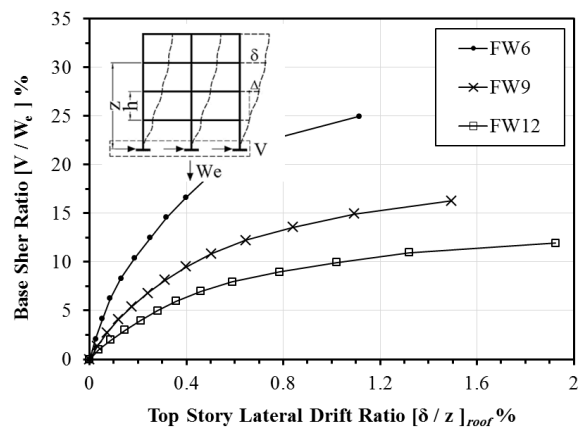


Figure 26: Base shear versus top story lateral drift ratios for FW systems.

6.4 Force Modification Factors

Structures subjected to earthquake actions deform in nonlinear pattern that leads to plastic hinges formation and consequently earthquake energy dissipation. As a result, the base shear could be reduced if the structure

is nonlinearly analyzed. This reduction is introduced in a factor called “Force reduction factor (R)”. According to ECP-201 [13], the strength reduction factor for ductile framed structures is 7 while for limited ductile frames or for structures provided with shear walls is 5. Estimating of force reduction factor “R” depends on the structure fundamental period [15], Figure 34. The force reduction factors using the principal of equal energy is calculated by equating the hatched areas of the force displacement relationship for the top story, Figure 35. The estimated strength reduction factors based on nonlinear static analysis of the structural systems demonstrated in the present parametric study are less than those provided by ECP-201 [13] as listed in Table 9. This could be related to the nonlinear static analysis was stopped when limit load is reached

Table 8: Predicted collapse base shear ratios for different systems.

Building Layout	Building Stories	Floor System	Collapse base shear ratio = (V/W_c)	Base shear ratio at 0.2% top story lateral drift ratio = (β)	$(V/W_c) / (\beta)$
FC6	6	Flat-Slab	14.1	4.82	2.92
FC9	9	Flat-Slab	11.5	3.34	3.44
FC12	12	Flat-Slab	9.1	2.40	3.80
FW6	6	Flat-Slab	25	10.82	2.31
FW9	9	Flat-Slab	16.2	5.95	2.73
FW12	12	Flat-Slab	11.9	3.81	3.12
SC6	6	Slab-Beam	21.1	15.4	1.37
SC9	9	Slab-Beam	17.2	11.13	1.54
SC12	12	Slab-Beam	13.9	8.4	1.65
SW6	6	Slab-Beam	50.5	32.4	1.56
SW9	9	Slab-Beam	32.2	19.5	1.65
SW12	12	Slab-Beam	22.6	13.40	1.68

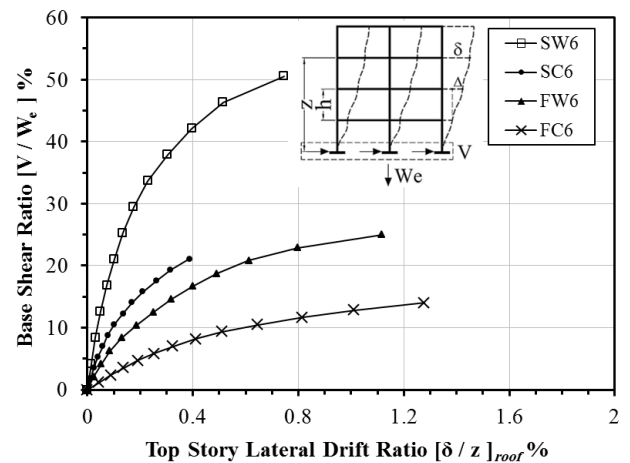


Figure 27: Base shear versus top story lateral drift ratios for 6 stories buildings.

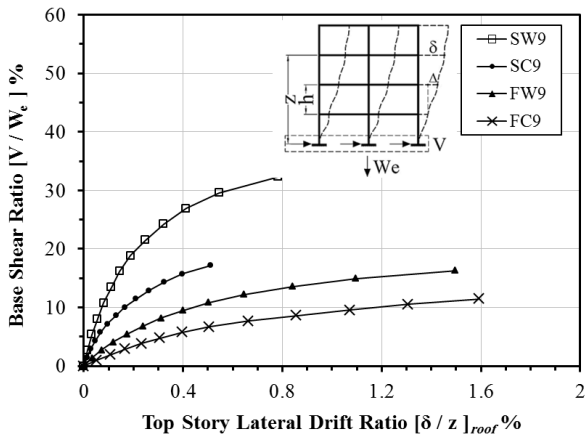


Figure 28: Base shear versus top story lateral drift ratios for 9 stories buildings.

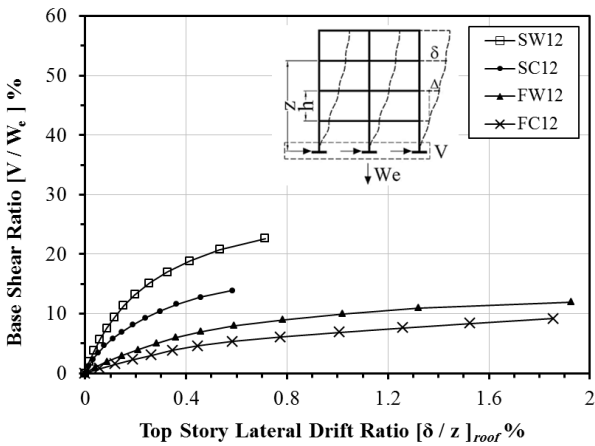


Figure 29: Base shear versus top story lateral drift ratios for 12 stories buildings.

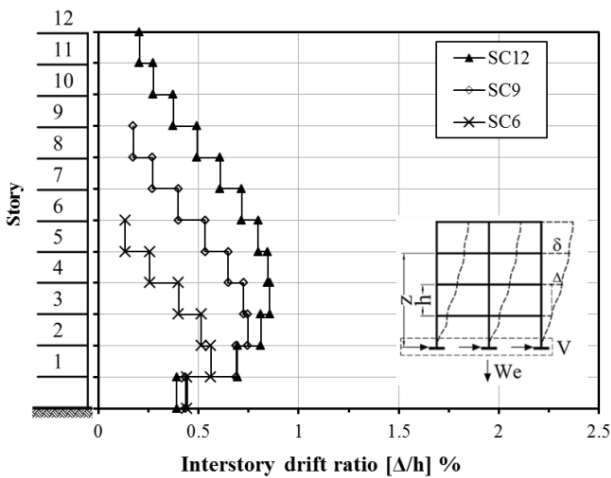


Figure 30: Interstory drift ratio prior to failure for system layout (SC).

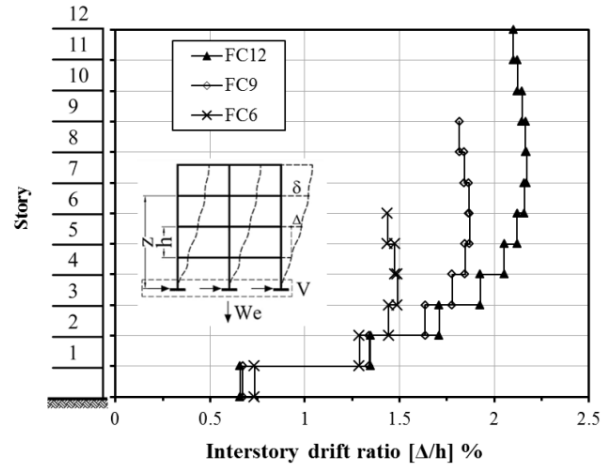


Figure 31: Interstory drift ratio prior to failure for system layout (FC).

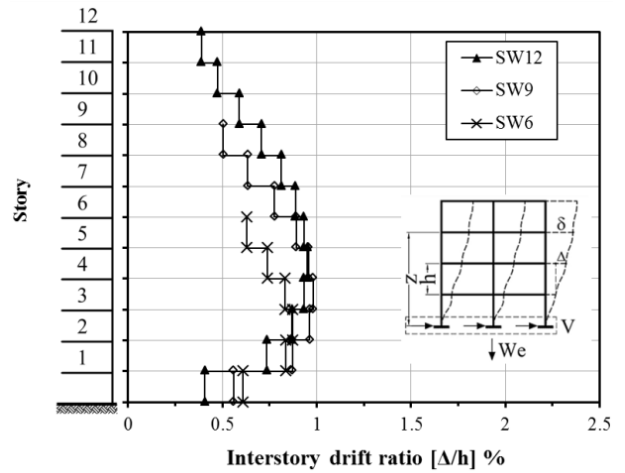


Figure 32: Interstory drift ratio prior to failure for system layout (SW).

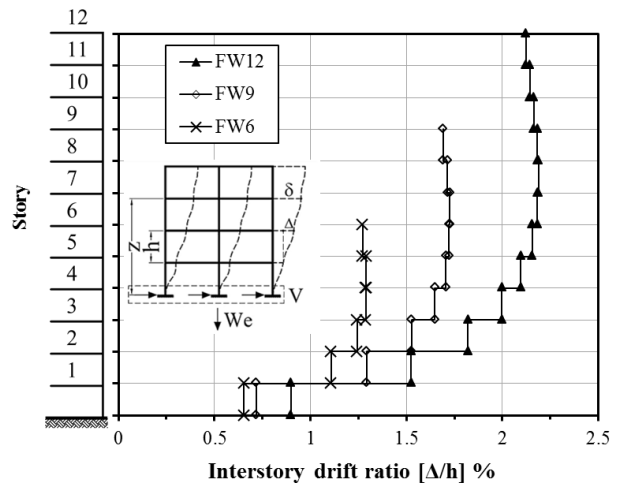


Figure 33: Interstory drift ratio prior to failure for system layout (FW).

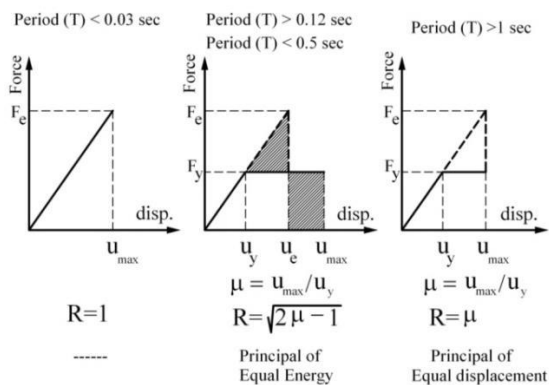


Figure 34: Force reduction factors [15]

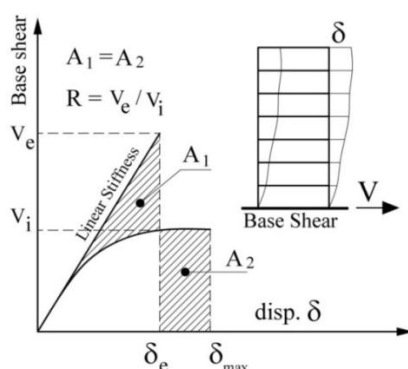


Figure 35: Force reduction factors from load displacement relationship

Table 9: Estimated force reduction factors (R).

Building Layout	Top story lateral drift from nonlinear analysis [m]	Nonlinear base shear capacity [kN] V_{NL}	Linear base shear causing same top story lateral drift [kN] V_L	$R = V_L / V_{NL}$	R (From Equal Energy)
SC6	0.074	800	2086	2.60	2.24
SC9	0.143	980	3077	3.14	2.51
SC12	0.216	1060	3470	3.27	2.60
FC6	0.244	504	1592	3.16	2.65
FC9	0.444	620	2037	3.29	2.62
FC12	0.680	658	2284	3.47	2.71
SW6	0.140	1920	7810	4.07	3.06
SW9	0.215	1840	7407	4.03	2.98
SW12	0.260	1720	5996	3.49	2.80
FW6	0.212	900	3620	4.02	2.9
FW9	0.420	880	3803	4.32	2.95
FW12	0.711	860	4178	4.86	3.20

7. Conclusions

An improved reinforced concrete plane stress element analysis technique is presented in the current study. The improved element is used in the nonlinear analysis of shear walls subjected to cyclic loading. Moreover, it is implemented into a finite element program in order to study the static response of case study with different seismic resisting system. The building vertical and floor elements were designed according to Egyptian codes for design and load calculations. For the sake of comparison, two types of floor systems in addition to two types of seismic resisting systems were nonlinearly analyzed using triangular lateral load pattern. Based on the current study, the following concluding remarks could be drawn.

1. Analysis of shear walls using membrane elements with the assumption of rotating crack must involve crack angle capturing algorithm as presented in the current study.
2. The behavior of seismic resisting systems subjected to lateral forces can be satisfactory captured, if nonlinear static analysis with the presence of vertical loads is performed.
3. With respect to top story drift limitation, if two systems were designed according to vertical and lateral loads one as flat slab and other as slab-beam, the collapse base shear for the slab-beam systems is about twice its value for the flat slab system.
4. In addition to interstory profile difference, the critical story (i.e. story at which maximum interstory drift is found) is located at about one third and one half building height for beamed slab and flat slab systems, respectively.
5. The estimated force reduction factors, based on nonlinear static analysis of the structural systems demonstrated in the examined systems in the current work, are 50% to 75% of those provided by Egyptian code [13]

8. References

- [1] Vecchio, F. J. (1986). The Modified Compression Field Theory for Reinforced Concrete Elements Subjected to Shear. ACI Journal, 219-231.
- [2] Vecchio, F. J. (1990). Reinforced Concrete Membrane Element Formulation. Journal of Structural Engineering, Vol.116, No. 3, 730-750.
- [3] Hut, H., & Schnobrich, W. C. (1991). Nonlinear Finite Element Analysis of Reinforced Concrete Plates and shells under Monotonic Loading. Computers & Structures Vol. 38, No. 516., 631-651.
- [4] Jagd, L. K. (1996). Nonlinear Seismic Analysis of RC Shear Wall. Denmark: PhD Report, Technical

university of Denmark, Department of Structural Engineering and Materials, Series R, No. 5.

- [5] Hidalgo, P. A., Jordan, R. M., & Martinez, M. P. (2001). An analytical model to predict the inelastic seismic behavior of shear-wall, reinforced concrete structures. *Engineering Structures*, 85-98.
- [6] Mo, Y., Zhongb, J., & Hsu, T. T. (2008). Seismic Simulation of RC Wall-type Structures. *Engineering Structures*, doi:10.1016 , 2008.04.033.
- [7] Rahal, K. N. (2010). Post-cracking shear modulus of reinforced concrete membrane elements. *Engineering Structures*, Vol. 32 , 218-225.
- [8] Kent, D., & Park, R. (1971). Flexural members with confined concrete. *Journal of the Structural Division, Proc. of the American Society of Civil Engineers*, 97, ST7, 1969-1990.
- [9] Hognestad, E. (1951). A study on combined bending and axial load in reinforced concrete members. Univ. of Illinois at Urbana-Champaign, IL, 43-46: Univ. of Illinois Engineering Experiment Station.
- [10] He, W., Wu, Y.-F., & Liew, K. (2008). A fracture energy based constitutive model for the analysis of reinforced concrete structures under cyclic loading. *Comput. Methods Appl. Mech. Engrg.*, 197 - p4745–4762, 197 (2008) 4745–4762.
- [11] Menegotto, M., & Pinto, P. E. (1973). Method of analysis for cyclically loaded R.C. plane frames including changes in geometry and non-elastic behavior of elements under combined normal force and bending. Roma, Italy: IABSE reports of the working commissions.
- [12] Oesterle, R., Fiorato, A., & Johal, L. (1976). Earthquake-resistant structural walls – Tests of isolated walls. Skokie, Illinois, 315pp.: National Science Foundation, Construction Technology Laboratories, Portland Cement Association.
- [13] ECP-201. (2012). Egyptian Code for Loads and Forces in Structures and Buildings. Cairo, Egypt.
- [14] ECP-203. (2007). Egyptian Code for Design and Construction of Reinforced Concrete Structures. Cairo, Egypt.
- [15] Newmark, N., & Hall, W. (1982). Earthquake spectra and design. Monograph Series, Oakland: EERI.